Few-nucleon scattering in pionless effective field theory

Martin Schäfer ●* and Betzalel Bazak ●†

The Racah Institute of Physics, The Hebrew University, Jerusalem 9190401, Israel

We present a comprehensive theoretical study of low-energy few-nucleon scattering for systems with $A \leqslant 4$. To this end, we utilize pionless effective field theory, which we employ at next-to-leading order. We show that at this level the theory yields accurate predictions for the low-energy scattering parameters in all studied channels. These predictions are on par with the best experimental evaluations and the available theoretical calculations. We confirm the recent observation that a four-body force is needed at next-to-leading-order and find that for nuclear systems it only appears in a single spin-isospin channel.

I. INTRODUCTION

Effective field theories (EFTs) provide a thorough framework for the study of low-energy physics. In nuclear physics, EFTs are low-energy manifestations of the underlying theory, quantum chromodynamics (QCD). As such, they are formulated in terms of baryons and mesons as the fundamental degrees of freedom, rather than quarks and gluons, and are constructed to obey the symmetries of QCD. For a recent review see, e.g., [1].

Of particular interest is pionless EFT ($\not\pi$EFT), which is the simplest possible nuclear EFT, having the mesons integrated out leaving the nucleons as the only degrees of freedom. $\not\pi$EFT is best suited to describe very low-energy processes and to explore universal physics, i.e., phenomena which are not sensitive to the details of the interparticle interaction and are therefore common to systems as different as nucleons and atoms. As the deuteron binding energy is unnaturally small, light nuclei belong to a universality class where the scattering length is much larger than the interaction range. For a large and positive scattering length, a bound dimer exists whose energy is almost entirely determined by the scattering length alone. Besides the deuteron, another natural example of such a dimer is the He$_2$ molecule.

Behind its apparent simplicity, $\not\pi$EFT, as is implied here, exhibits some peculiar features, such as (a) the Wigner bound, which limits the possible values of the effective range and thus forces a perturbative treatment of all but leading-order (LO) terms [2]; (b) the Thomas collapse, compelling the promotion of a three-body contact term to LO [3,4]; (c) the Efimov effect [5], dictating the three-body states binding energy; and (d) the appearance of a four-body force at next-to-leading-order (NLO) [6]. Here, we would like to test the utility of $\not\pi$EFT, comparing the predictions of the theory at NLO to experimentally measured low-energy two-clusters *s*-wave scattering

data of reactions involving $A \leqslant 4$ nucleons. To be more specific, as we use the $A = 2$ nucleon-nucleon ($N + N$) scattering lengths and effective ranges, as well as the triton binding energy, to fit the low-energy constants (LECs) of the theory, we test $\not\pi$EFT ability to predict the three-body $N + 2N$, and the four-body $2N + 2N$, and $N + 3N$ low-energy scattering parameters.

The application of $\not\pi$EFT to study low-energy scattering dates back to its first days [7,8]. However, so far, published works were predominantly limited to nuclear systems with $A \leqslant 3$, i.e., nucleon-nucleon or nucleon-deuteron scattering. Here, we extend these studies considering perturbative insertion of next-to-leading order (NLO) terms and describing most *s*-wave scattering processes with $A \leqslant 4$.

When the scattering length is much larger than the interaction range, three identical bosons in an *s* wave exhibit the Efimov effect. In the corresponding spin-half fermionic system, three particles in a relative *s* wave are blocked due to the Pauli principle, and therefore Efimov effect appears only in higher partial waves [9–11]. Scattering of an atom from fermionic dimer, however, exhibits universal characteristic, and the atom-dimer scattering length a_{a-dm} is determined by the atom-atom scattering length a_{aa}, $a_{a-dm} \approx 1.2a_{aa}$ [12–14]. Moreover, the dimer-dimer scattering length is also universal and $a_{dm-dm} \approx 0.6a_{aa}$ [15].

In nuclear physics, where the nucleons carry two internal degrees of freedom, spin and isospin, both phenomena are relevant. In some cases, three or four nucleons have symmetric spatial wave functions and therefore behave like a bosonic system, while in other cases they have an antisymmetric one and thus behave like fermions, depending on the quantum numbers. To see that, let us consider three nucleons with zero total orbital angular momentum. In the spin-isospin $S, I = (1/2, 1/2)$ channel, the nucleons behave like bosons and therefore bound Efimovian three-body state exists and a three-body force is to be introduced to set its energy [4]. In contrast, neutron-deuteron scattering in the $S, I = (3/2, 1/2)$ channel is subject to Pauli blocking, and therefore universal fermionic behavior is expected [12].

*schafer.martin@mail.huji.ac.il
†betzalel.bazak@mail.huji.ac.il

064001-1

This is also the case for the four nucleon system. While deuteron-deuteron scattering in the $S, I = (2, 0)$ channel has a fermionic nature, the $S, I = (0, 0)$ channel is bosonic and a bound four-body state exists, i.e., ^{4}He. This channel is of particular interest since it was shown recently that for a bosonic system, a four-body force must be introduced at NLO to regularize the system [6]. It is therefore interesting to check if such a force is needed also in the nuclear case, and if so in which channels.

Several studies have applied $\not{\pi}$EFT to the *nd* scattering [7,8,16–24]. The spin-quartet *s*-wave channel was studied in Refs. [7,8], resuming effective-range corrections to all orders. The calculated *nd* scattering length was found to be 6.33 fm, in excellent agreement with the experimental value 6.35(2) fm [25]. The calculated phase shifts agreed with the phase shift analysis of Refs. [26,27]. In the $S, I = (1/2, 1/2)$ channel, a three-body parameter is needed and can be fitted, for example, to the triton binding energy. Perturbative range corrections in this channel were considered in Ref. [18], and they were followed by calculations of higher-order contributions in [19,20]. A fully perturbative study of *nd* scattering up to N^{2}LO was done in Ref. [21], in a way that does not require the calculation of the full off-shell scattering amplitude, needed in earlier studies [28,29]. In the presence of Coulomb interaction, *pd* scattering was studied as well [30–32].

So far, four-nucleon scattering has not been explored extensively within the framework of $\not{\pi}$EFT. The $p\,^3$He and *nt* scattering lengths were calculated at LO in Ref. [33]. While the $p\,^3$He results were burdened by relatively large theoretical errors, the predicted *nt* scattering lengths were found to be somewhat smaller than a compilation of phenomenological results presented there. A calculation of the spin-singlet $n\,^3$He scattering length was performed in Ref. [34] using a nonperturbative $\not{\pi}$EFT NLO potential.

Here, we present a systematic study of low-energy nuclear scattering up to $A \leqslant 4$. We calculate scattering lengths and effective ranges for all available spin-isospin channels, to second order in $\not{\pi}$EFT. To this end, we apply a shallow harmonic oscillator trap to the studied system, and extract the corresponding scattering parameters using the Busch formula [35,36]. Bound-state energies and wave functions with and without the trap are obtained employing a correlated Gaussian basis with the stochastic variational method (SVM) [37].

The paper starts with a short description of $\not{\pi}$EFT in Sec. II. In Sec. III we present the numerical tools applied in our work. The fitting of $\not{\pi}$EFT low-energy constants is briefly described in Sec. IV. The results for different few-nucleons channels are presented in Sec. V, followed by our conclusions in Sec. VI.

II. MODEL

In this work, we study the few-nucleons scattering in the framework of $\not{\pi}$EFT. The dynamical degrees of freedom are nucleons, while pions, as well as other degrees of freedom, are integrated out, and the corresponding physics is encapsulated in the low energy constants.

Since EFT contains all terms consistent with the symmetries of the underlying theory, a power counting, i.e., a scheme to determine which terms belong to each order of the theory,

must be introduced in order to restore its predictive power. Naive power counting suggests only two-body *s*-wave contact interactions at LO, and therefore the relevant Lagrangian density should be

$$\mathcal{L}_{\text{LO}} = N^\dagger \left(i\partial_0 + \frac{\nabla^2}{2m} \right) N - \frac{1}{2} C_0^{(0)} \left(N^\dagger \hat{\mathcal{P}}_{2b}^{0,1} N \right)^2$$
$$- \frac{1}{2} C_1^{(0)} \left(N^\dagger \hat{\mathcal{P}}_{2b}^{1,0} N \right)^2. \tag{1}$$

Here, we set $\hbar = 1$, N is the nucleon field operator and m its mass, $\hat{\mathcal{P}}_{2b}^{S,I}$ is a projection operator on a two-body channel with spin S and isospin I, $C_0^{(0)}$ and $C_1^{(0)}$ are the low-energy constants.

In the three-body spin-isospin $S, I = (1/2, 1/2)$ channel all nucleons can occupy the *s* shell and the system collapses [3]. As a result, a three-body contact term must be introduced [4],

$$\mathcal{L}_{\text{LO}}^{(3b)} = -\tfrac{1}{6} D^{(0)} \left(N^\dagger \hat{\mathcal{P}}_{3b}^{1/2,1/2} N \right)^3, \tag{2}$$

where $D^{(0)}$ is the three-body LEC and $\hat{\mathcal{P}}_{3b}^{S,I}$ is a projection operator into a tree-body spin-isospin channel.

At LO, the interaction is to be iterated, which is equivalent to solving the nonrelativistic Schrödinger equation with the Hamiltonian

$$H_{\text{LO}} = -\frac{1}{2m} \sum_i \nabla_i^2 + V_2^{(0)} + V_3^{(0)}, \tag{3}$$

where $V_2^{(0)}$ and $V_3^{(0)}$ are LO two- and three-body contact potentials, respectively.

The singular nature of contact interactions requires regularization, which is performed here by applying a local Gaussian regulator that suppresses momenta above an ultraviolet cutoff. Physical quantities predicted by the theory have to be independent of the cutoff since it is not physical quantity. This is achieved via renormalization, i.e., by fitting the values of the LECs to run with the cutoff in such a way that a chosen set of physical observables is reproduced. The regularized LO two-body potential then is

$$V_2^{(0)} = \sum_{i<j} \left(C_0^{(0)} \hat{\mathcal{P}}_{ij}^{0,1} + C_1^{(0)} \hat{\mathcal{P}}_{ij}^{1,0} \right) g_\lambda(r_{ij}), \tag{4}$$

and the three-body potential is

$$V_3^{(0)} = D_0^{(0)} \sum_{i<j<k} \sum_{\text{cyc}} \hat{\mathcal{P}}_{ijk}^{1/2,1/2} g_\lambda(r_{ij}) g_\lambda(r_{ik}), \tag{5}$$

where $g_\lambda(r) \propto \exp(-\lambda^2 r^2/4)$ is the chosen regulator, *cyc* denotes the cyclic sum, and $r_{ij} = |\mathbf{r}_i - \mathbf{r}_j|$ is a relative distance between nucleons i and j. As $\lambda \to \infty$, the contact nature of the interaction is recovered.

The next-to-leading order contains range corrections, with new LECs $C_2^{(1)}$ and $C_3^{(1)}$ to be determined from two-body

observables. The corresponding potential can be written as

$$V_2^{(1)} = \sum_{i<j} \left(C_2^{(1)} \hat{\mathcal{P}}_{ij}^{0,1} + C_3^{(1)} \hat{\mathcal{P}}_{ij}^{1,0} \right) \left(g_\lambda(r_{ij}) \overrightarrow{\nabla}_{ij}^2 + \overleftarrow{\nabla}_{ij}^2 g_\lambda(r_{ij}) \right).$$

(6)

Unlike the LO interaction, which has to be treated nonperturbatively, NLO consists of a single insertion of the potential. Renormalization cannot be achieved for a positive effective range when an inconsistent subset of higher-order corrections is included by the nonperturbative solution of the Schrödinger equation with the NLO potential [38]. Note that only recent studies of ꬰEFT scattering indeed treat NLO terms perturbatively.

Perturbative inclusion of range corrections, Eq. (6), changes renormalization conditions used at LO. As a result one has to consider perturbative inclusion of counterterms in a form equivalent to Eqs. (4) and (5). This ensures that the renormalization conditions applied at LO remain satisfied at NLO and it leads to three other LECs—$C_1^{(1)}$, $C_2^{(1)}$, and $D_0^{(1)}$.

For a bosonic case, it was shown recently that a contact four-body term has to be added at NLO [6]. In this work, we demonstrate that indeed this is also the case for nuclei and a four-body term has to be considered in the $S, I = (0, 0)$ four-body channel to obtain reasonable results at this order. Here, we use hyper-radial four-body force

$$V_4 = E_0^{(1)} \sum_{i<j<k<l} \hat{\mathcal{P}}_{ijkl}^{0,0} g_\lambda(r_{ijkl}),$$

(7)

where r_{ijkl} is the four particles hyper-radius, $r_{ijkl}^2 = \sum_{\mu<\nu \in \{i,j,k,l\}} r_{\mu\nu}^2$, and $E_0^{(1)}$ denotes four-body LEC. Note, that the more economical hyper-radial form of the four-body force was chosen over the one using a cyclic sum which includes many permutations.

III. METHOD

Few-body bound-state solutions are obtained by expanding the corresponding wave function Ψ in a correlated Gaussian basis,

$$\Psi = \sum_i c_i \hat{\mathcal{A}} \exp\left(-\frac{1}{2} \mathbf{x}^T \mathbf{A}_i \mathbf{x} \right) \chi_{SM_S}^i \xi_{IM_I}^i,$$

(8)

where the operator $\hat{\mathcal{A}}$ ensures antisymmetrization between nucleons, $\mathbf{x}^T = (\mathbf{x}_1, \ldots, \mathbf{x}_{A-1})$ is a set of Jacobi coordinates, and $\chi_{SM_S}^i$ and $\xi_{IM_I}^i$ stand for the relevant spin and isospin parts, respectively. Here, $\mathbf{A}_i$ is an $(A-1) \times (A-1)$ positive-definite symmetric matrix with $A(A-1)/2$ nonlinear parameters. Both bound-state energies and variational parameters c_i are obtained by diagonalizing the Hamiltonian matrix. In order to choose basis states with the most appropriate nonlinear parameters, we use the SVM [37], which was proved to offer an effective procedure to optimize the finite basis set, yielding a very accurate description of bound states.

Scattering states are not compact in space, which makes them more difficult to calculate. As a result, it might be easier to extract scattering parameters from bound-state calculations. To do so, one can apply periodic boundary conditions to the system at hand, calculate the discrete energies for a few

box sizes, and then use the Lüscher formulas to extract the scattering parameters in free space [39].

A similar approach, which we use here, is to trap the studied nuclear A-body system in a harmonic oscillator (HO) potential

$$V_{\text{HO}}(\mathbf{r}) = \frac{m}{2A} \omega^2 \sum_{i<j} (\mathbf{r}_i - \mathbf{r}_j)^2$$

(9)

with oscillator frequency ω. Consider the scattering of two bound subclusters B and C, and using a trap with length $b_{\text{HO}} = \sqrt{2/(m\omega)}$ much larger than the other length scales of the system, the subclusters then can be considered as point-like particles. As a result, one can match the asymptotic part of the trapped wave function to the known solution of two trapped particles with a short-range interaction. The BC phase shifts δ_{BC} at relative momentum k then can be extracted using the Busch formula [35,36]

$$-\sqrt{4\mu\omega} \frac{\Gamma(3/4 - \epsilon_\omega^n/2\omega)}{\Gamma(1/4 - \epsilon_\omega^n/2\omega)} = k \cot \delta_{BC},$$

(10)

where $\mu = m_B m_C/(m_B + m_C)$ is the BC reduced mass, $\Gamma(x)$ is the Gamma function, $k = \sqrt{2\mu\epsilon_\omega^n}$, and $\epsilon_\omega^n = E_\omega^n(A) - E_\omega(B) - E_\omega(C)$ is the nth excited state energy of the trapped A-body system with respect to the $B + C$ threshold. Here, bound-state energies $E_\omega(B)$, $E_\omega(C)$, and $E_\omega^n(A)$ are calculated using the SVM. Throughout this work $BC \in \{NN, nd, nt, n^3\text{He}, dd\}$ and all phase shifts are extracted applying HO trap lengths $15\,\text{fm} \leqslant b_{\text{HO}} \leqslant 50\,\text{fm}$.

Note that one should consider energy levels above the trapped $B + C$ threshold disregarding possible BC bound states. If there are any higher thresholds corresponding to further disintegration of B or C subclusters we select only such levels which correspond to BC scattering in the HO trap.

The scattering length a_{BC} and effective range r_{BC} then result from fitting the calculated phase shifts with the effective range expansion (ERE)

$$k \cot \delta_{BC} = -\frac{1}{a_{BC}} + \frac{1}{2} r_{BC} k^2 + \ldots.$$

(11)

Next-to-leading order bound-state energies are obtained considering a single insertion of the NLO potential. Using first-order perturbation theory,

$$E^{\text{NLO}} = E^{\text{LO}} + \frac{\langle \Psi^{\text{LO}} | V^{\text{NLO}} | \Psi^{\text{LO}} \rangle}{\langle \Psi^{\text{LO}} | \Psi^{\text{LO}} \rangle},$$

(12)

where V^{NLO} stands for the sum of all NLO potential terms and Ψ^{LO} is the LO bound-state wave function. Scattering predictions at NLO are calculated by changing the trapped energies, using first-order perturbation theory, Eq. (12), and then applying Eq. (10) to extract the scattering parameters [40,41]. This way one can avoid calculating the off-shell scattering matrix while still taking NLO in a perturbative way.

Since Eq. (10) relies on the difference between energies in shallow traps, the corresponding values should be calculated with high precision. To do so we first use SVM to build several basis sets, each optimized for different trap lengths and cutoffs. These basis sets are then joined into a larger basis
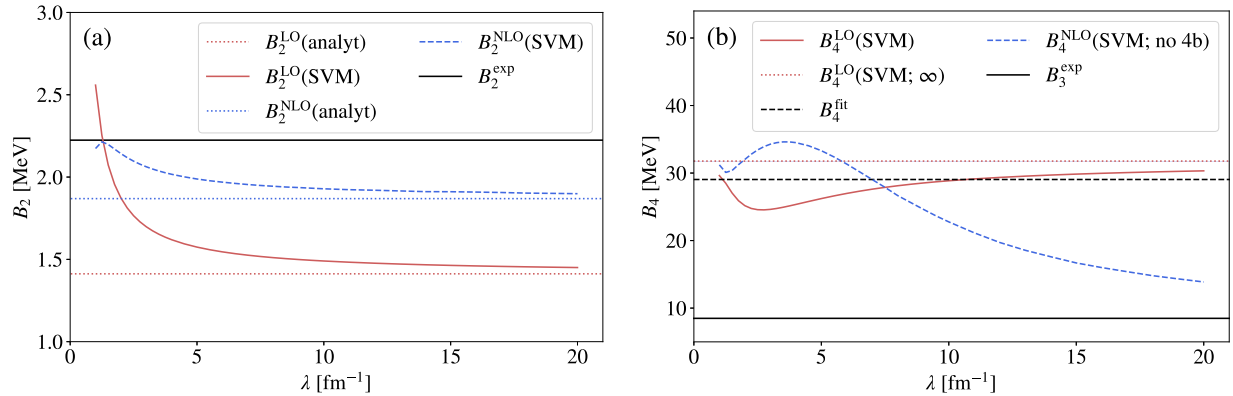
FIG. 1. (a) The deuteron binding energy as a function of the cutoff λ. The $B_2^{\text{LO}}(\text{SVM})$ and $B_2^{\text{NLO}}(\text{SVM})$ denote LO and NLO binding energies calculated using SVM. The $B_2^{\text{LO}}(\text{analyt})$ and $B_2^{\text{NLO}}(\text{analyt})$ values are predictions of Eq. (13). (b) The ^{4}He binding energy as a function of the cutoff λ. The $B_4^{\text{LO}}(\text{SVM})$ and $B_4^{\text{NLO}}(\text{SVM; no 4b})$ denote LO and NLO binding energies calculated using SVM with no four-body force considered at NLO. The $B_4^{\text{LO}}(\text{SVM}; \infty)$ stands for LO $\not\pi$EFT binding energy extrapolated to $\lambda \rightarrow \infty$ using $B_4(\lambda) = B_4(\infty) + \alpha/\lambda$ function. The B_4^{fit} shows experimental ^{4}He binding energy with Coulomb energy subtracted which is used to fix the NLO four-body force. The experimental triton binding energy B_3^{exp} is shown for comparison.

while omitting those states which are nearly linear dependent to maintain the numerical stability [42]. Checking the convergence of the bound-state energies $E_\omega^n(A)$, $E_\omega(B)$, and $E_\omega(C)$, as well as NLO expectation values with an increasing amount of basis states, we verify that the overall accuracy is below 10^{-4} MeV.

IV. FITTING THE EFT

Setting the numerical tools, we can fit the $\not\pi$EFT LECs to reproduce relevant experimental observables.

The LO potential, Eq. (3), has two two-body LECs, $C_0^{(0)}$ and $C_1^{(0)}$, corresponding to two s-wave NN channels, spin-singlet ($^1S_0$), and spin-triplet ($^3S_1$). We fit these LECs to reproduce the experimental spin-singlet neutron-neutron scattering length $a_{nn}^0 = -18.95$ fm [43,44] and spin-triplet proton-neutron scattering length $a_{pn}^1 = 5.419$ fm [45], respectively. Since LO terms are iterated to all orders, one can apply standard tools to calculate the scattering length; we use the variable phase method [46] as well as extracted it from phase shifts calculated with the Numerov method.

At NLO, each two-body channel has a new momentum-dependent term, Eq. (6), thus the effective ranges can be reproduced as well. Since NLO terms have to be treated perturbatively, we utilize the distorted-wave Born approximation (DWBA) to fit the LECs. To preserve leading order renormalization conditions, we consider a perturbative correction to the LO interaction. This results in two LECs in the NN $^1S_0$ channel, $C_0^{(1)}$ and $C_2^{(1)}$, and two LECs in the NN $^3S_1$ channel, $C_1^{(1)}$ and $C_3^{(1)}$, fitted to reproduce experimental neutron-neutron spin-singlet effective range $r_{nn}^0 = 2.75$ fm [47] and proton-neutron spin-triplet effective range $r_{pn}^1 = 1.753$ fm [45], respectively, while keeping the same values of scattering lengths as have been fitted at LO.

As we fit the two-body potential to scattering data, the deuteron binding energy B_2 is a prediction of the EFT. In the left panel of Fig. 1 we show LO and NLO B_2 values calculated via SVM as a function of the cutoff. For zero-range attractive

interaction, the LO and NLO deuteron binding energy can be calculated analytically

$$B_2^{\text{LO}} = \frac{1}{m(a_{NN}^1)^2}, \quad B_2^{\text{NLO}} = B_2^{\text{LO}}\left(1 + \frac{r_{NN}^1}{a_{NN}^1}\right). \quad (13)$$

Corresponding binding energy values are shown as red (LO) and blue (NLO) dotted lines in Fig. 1(a). Clearly, our SVM results converge to these values as $\lambda \longrightarrow \infty$.

To constrain the LO three-body term we use SVM to solve for the triton binding energy and fit its $D_0^{(0)}$ LEC to reproduce the experimental value, $B_3 = 8.482$ MeV [48]. Although no new three-body term appears at NLO, the LO term has to be corrected by introducing a three-body counterterm. Using the LO triton wave function, the corresponding LEC $D_0^{(1)}$ is fitted perturbatively keeping the NLO triton binding energy at its experimental value, while inserting the two-body NLO interaction.

At LO, the ^{4}He binding energy B_4 is correlated to that of the triton, and thus no four-body force is needed. However, it was shown recently [6] that this is not the case at NLO for a bosonic system, where a contact four-body term has to be added to regularize the four boson system. Here, we show that this is also the case for nuclei. Figure 1(b) shows B_4 as a function of the cutoff. The LO results, calculated via SVM, indeed converge at large λs to a reasonable value. However, the perturbative inclusion of NLO corrections without the four-body force gives much smaller binding energy. One should notice that for $\lambda \geqslant 10$ fm^{-1} such NLO corrections induce change larger than 30% with respect to the LO result which casts certain doubts on the validity of a perturbative approach. Furthermore, while it is generally expected that residual cutoff dependence will decrease with the inclusion of higher orders, our findings indicate the opposite trend. This applies not only to the results presented here, but also to similar results for $N + 3N$ scattering in the same channel. This reveals the necessity of a four-body force, Eq. (7), at NLO. Its LEC $E_0^{(1)}$ is perturbatively fitted, using SVM LO ^{4}He wave
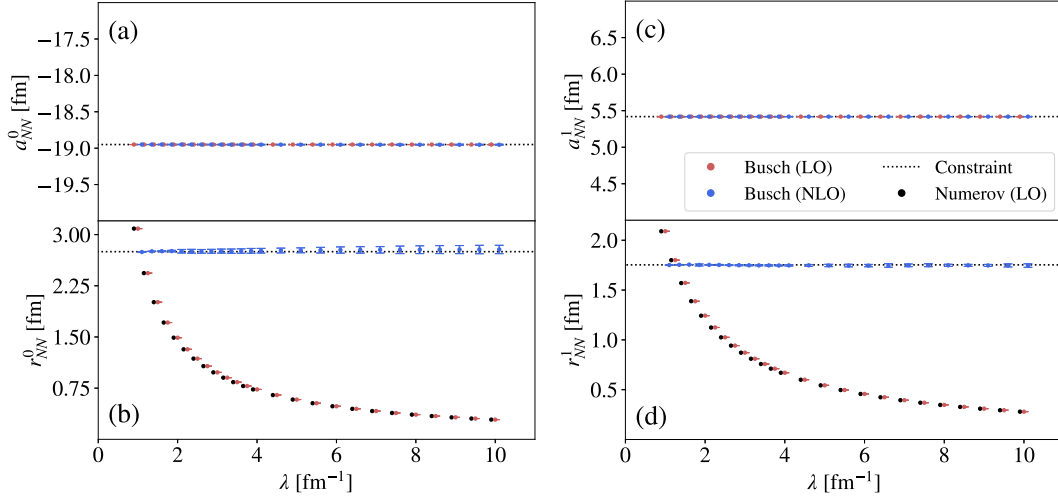
FIG. 2. Left side: Spin-singlet NN scattering length a_{NN}^0 (a) and effective range r_{NN}^0 (b) values extracted from LO (red) and NLO (blue) phase shifts calculated via Busch formula, Eq. (10), as a function of increasing momentum cutoff λ. Dotted lines show experimental a_{NN}^0 and r_{NN}^0 constraints used to fix LO and NLO LECs. Black dots stand for LO r_{NN}^0 calculated via the Numerov algorithm. All LO Busch results are slightly shifted to the right in order to avoid complete overlap by displaying Busch NLO a_{NN}^0 and Numerov LO r_{NN}^0 results. Right side: The same as in the left panel but for spin-triplet NN channel.

function to get $B_4 = 29.046$ MeV [49], corresponding to the experimental value with Coulombic energy subtracted.

V. RESULTS

Equipped with the tools needed to study few-nucleon elastic scattering, we performed accurate calculations for $A \leqslant 4$ nuclear systems within LO and NLO $\not\pi$EFT. Considering a wide range of momentum cutoffs $\lambda \in [1, 10]\,\mathrm{fm}^{-1}$ we assess the cutoff dependence of our results, which also enable us to estimate the truncation error at each order by the residual cutoff dependence [50]. Our predictions are then thoroughly compared to the available experimental data.

A. Two nucleons

To check our numerical procedure, we consider two-nucleon s-wave scattering in the $^1S_0$ and $^3S_1$ channels. As mentioned above, corresponding experimental values of scattering lengths and effective ranges are used as an input to fit LO and NLO two-body LECs, respectively. We calculate here the low-energy scattering parameters from the phase shift extracted from SVM energies in a harmonic trap using the Busch formula.

In Figs. 2(a) and 2(b) we show the NN spin-singlet scattering length and effective range values, respectively, calculated using the Busch formula as a function of the momentum cutoff λ. Equivalent results for spin-triplet channel are in Figs. 2(c) and 2(d). For LO $\not\pi$EFT potential, we obtain cutoff independent scattering length values in agreement with experimental constraints used in the LO fit. As we approach the limit of zero-range interaction $\lambda \to \infty$, the effective ranges r_{NN}^0 and r_{NN}^1 converge to zero. Direct comparison between their residual values calculated at finite $\lambda \in [1, 10]\,\mathrm{fm}^{-1}$ using the Busch formula and those extracted using the Numerov algorithm reveals basically identical results.

Including perturbative NLO terms into the Busch formula yields the same values of scattering lengths as at LO. Calculated effective ranges, r_{NN}^0 and r_{NN}^1, are at NLO cutoff independent and in agreement with corresponding experimental values which have been used to fix $C_0^{(1)}$, $C_1^{(1)}$, $C_2^{(1)}$, and $C_3^{(1)}$ LECs via the distorted-wave Born approximation.

B. Three nucleons

For a system of three nucleons, there are two spin-isospin channels $S, I = (1/2, 1/2)$ (doublet) and $S, I = (3/2, 1/2)$ (quartet) which describe s-wave elastic scattering between deuteron bound state and the remaining nucleon. In all other channels, there is no two-body bound state.

1. Doublet channel (S = 1/2)

In the spin-doublet channel, all nucleons are allowed to occupy the s shell, and thus a three-body repulsive force is needed to prevent the Thomas collapse [3,4].

A characteristic feature here is the presence of a node in the S matrix located close to the threshold. This leads to an anomalous behavior of corresponding scattering phase shifts: once displayed in terms of $k \cot \delta_{nd}^{1/2}$ as a function of nd relative momentum squared k^2 they are dominated by the presence of a pole and conventional ERE does not apply. Hence, one must consider the modified effective range expansion [26]

$$k \cot \delta_{nd}^{1/2} = -A + \frac{B}{2}k^2 - \frac{C}{1 + Dk^2} + \dots, \quad (14)$$

where $a_{nd}^{1/2} = 1/(A + C)$, $r_{nd}^{1/2} = B$, and the last term accounts for a pole position at $k^2 = -1/D$.

We calculate the spin-doublet nd scattering phase shifts at LO and NLO for different momentum cutoffs λ. Inspection of the corresponding $k \cot \delta_{nd}^{1/2}$ values reveals considerable dependence on the nd relative momentum k^2 in agreement
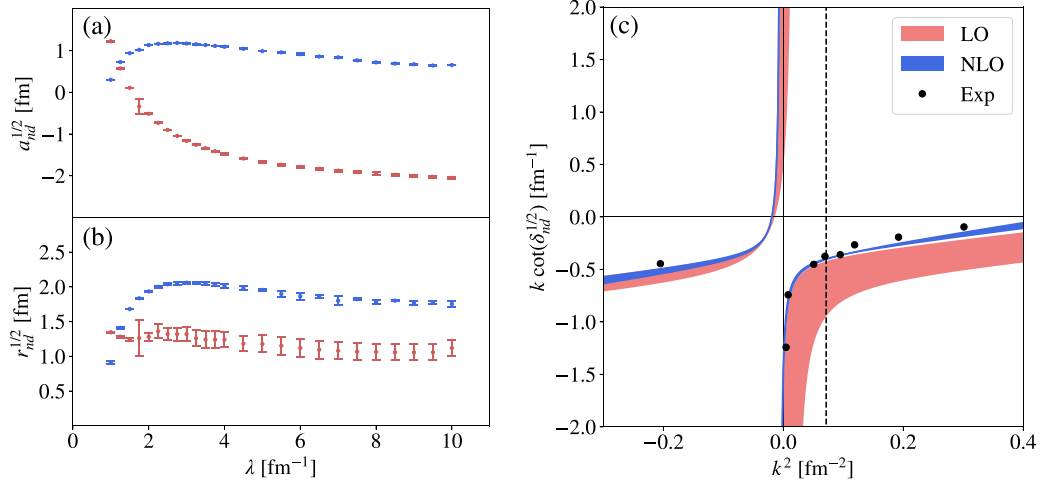
FIG. 3. Left side: Spin-doublet nd scattering lengths $a_{nd}^{1/2}$ (a) and effective ranges $r_{nd}^{1/2}$ (b) at LO (red) and NLO (blue), extracted using modified ERE, Eq. (14), as a function of increasing momentum cutoff λ. (c) Possible LO (red) and NLO (blue) $k \cot \delta_{nd}^{1/2}$ values suggested by cutoff variation for $\lambda \in [1.25, 10]$ fm^{-1}. Black dots represent experimental phase shifts from Ref. [26], the $k^2 < 0$ point relates to the triton bound state. A dashed black vertical line marks the deuteron breakup threshold.

with the pole structure assumed in Eq. (14). In order to explore the effect of the pole on the nd scattering, we fit calculated LO and NLO $k \cot \delta_{nd}^{1/2}$ values using Eq. (14). At LO, the pole position moves quite rapidly with an increasing cutoff from the subthreshold region $k^2 < 0$ above the nd threshold $k^2 > 0$ and starts to converge at $\lambda \geqslant 4$ fm^{-1}. The inclusion of NLO corrections stabilizes the pole position just below the nd threshold. In Fig. 3(c) we show possible $k \cot \delta_{nd}^{1/2}$ values given by a residual cutoff dependence for $\lambda \in [1.25, 10]$ fm^{-1}. One can see that once NLO corrections are included, a good agreement of our results with the experimental data [26] is achieved.

The LO and NLO $a_{nd}^{1/2}$ and $r_{nd}^{1/2}$ values, extracted from the fit via Eq. (14), are shown as a function of the cutoff in Figs. 3(a) and 3(b), respectively. Larger uncertainties in LO $r_{nd}^{1/2}$ results are induced by the dominance of the pole term in the modified ERE in a small momentum region between the nd threshold and the deuteron breakup threshold. Considering residual cutoff variation for $\lambda \in [1.25, 10]$ fm^{-1} and the numerical accuracy of our results, we obtain

$$\text{LO}: a_{nd}^{1/2} = -0.9(1.5) \, \text{fm}, \quad r_{nd}^{1/2} = 1.20(26) \, \text{fm},$$

$$\text{NLO}: a_{nd}^{1/2} = 0.92(29) \, \text{fm}, \quad r_{nd}^{1/2} = 1.74(33) \, \text{fm}.$$

Having access to the fitted parameters of Eq. (14), we search for roots of the equation $k \cot \delta_{nd}^{1/2} - ik = 0$. This provides us with a momentum $\gamma_{nd}^{1/2}$ of the first triton excited state which we find in a form of near-threshold virtual state (Re$(\gamma_{nd}^{1/2}) = 0$; Im$(\gamma_{nd}^{1/2}) < 0$). In Fig. 4 we show Im$(\gamma_{nd}^{1/2})$ results at LO and NLO as a function of λ. Including NLO corrections largely suppresses a residual cutoff dependence. Taking into account numerical accuracy and λ variation we obtain at LO Im$(\gamma_{nd}^{1/2}) = 0.117(19)$ fm^{-1} and at NLO Im$(\gamma_{nd}^{1/2}) = 0.1271(39)$ fm^{-1}, corresponding to energies of $E_{nd}^{1/2} = -0.43(14)$ MeV and $E_{nd}^{1/2} = -0.503(31)$ MeV, respectively. Our results agree rather well with LO $\not{\pi}$EFT

prediction $E_{nd}^{1/2} = -0.574$ MeV of Ref. [24] and energy predicted by a separable potential model $E_{nd}^{1/2} = -0.48$ MeV [51].

2. Quartet channel (S = 3/2)

In the spin-quartet channel, two nucleons are allowed to occupy the s shell forming $S = 1$ deuteron bound state. The third nucleon is Pauli blocked preventing Thomas collapse and thus no three-body repulsive force is necessary. Moreover, LO and NLO potentials, Eqs. (4),(6), contribute to this channel only through s-wave spin-triplet two-body interaction which provides us with a resemblance to a fermionic atom-dimer scattering.

The LO nd spin-quartet phase shifts $k \cot \delta_{nd}^{3/2}$ in the zero-range limit can be obtained straightforwardly solving the
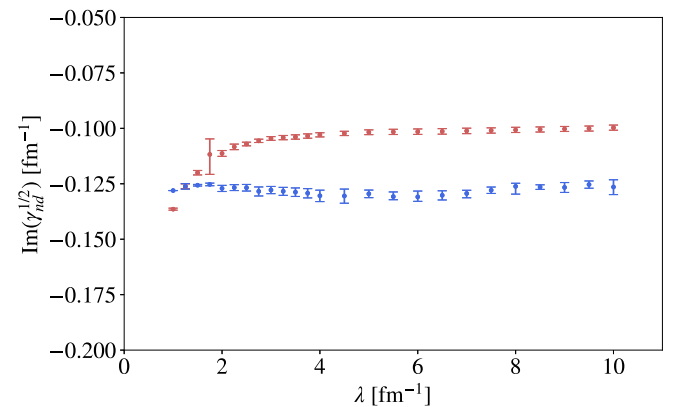

FIG. 4. Imaginary part of the triton virtual state momentum Im$(\gamma_{nd}^{1/2})$ as a function of momentum cutoff λ obtained as a root of $k \cot \delta_{nd}^{1/2} - ik = 0$. Here, $k \cot \delta_{nd}^{1/2}$ is represented by modified ERE, Eq. (14), and fitted to calculated LO (red) and NLO (blue) nd phase shifts in $S = 1/2$ s-wave channel.
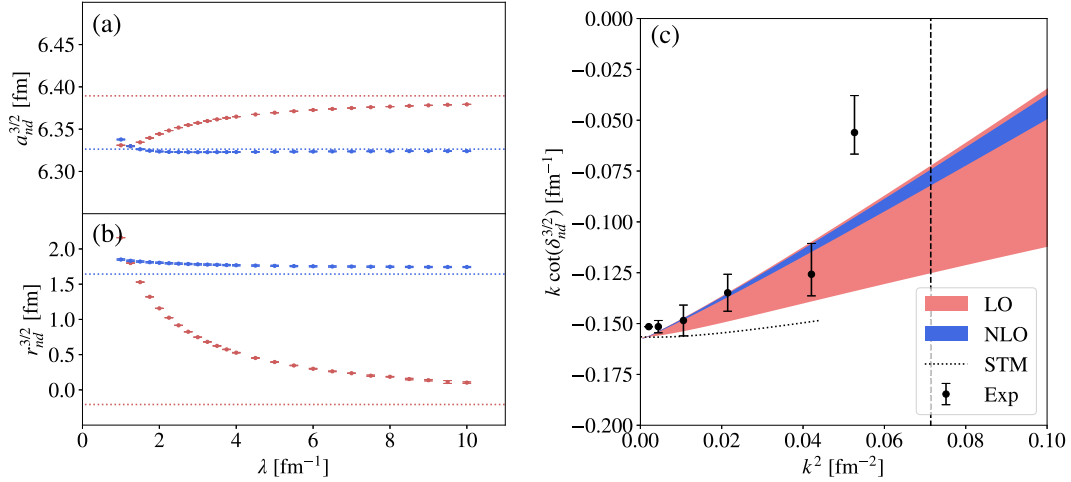
FIG. 5. The same as Fig. 3, but for spin-quartet nd scattering. In (a) and (b), red dotted lines show STM [12] $a_{nd}^{3/2}$ and $r_{nd}^{3/2}$ zero-range predictions. Blue dotted lines show $a_{nd}^{3/2}$ and $r_{nd}^{3/2}$ values calculated using universal fermionic atom-dimer relations in Eqs. (15) and (16). Black error bars in (c) represent experimental phase shifts from Ref. [27]. The dotted black line in the same panel shows scattering prediction at the zero-range limit obtained by solving the STM equation [12].

Skorniakov-Ter-Martirosian (STM) equation [12]. The corresponding results are depicted using a black dotted curve in Fig. 5(c). Starting at $k = 0$ calculated STM $k \cot \delta_{nd}^{3/2}$ values first decrease with increasing k^2 and then start to raise at very small momentum value $k^2 \approx 0.003$ fm^{-2}. This is a signature of negative effective range as well as significantly restricted convergence radius of ERE with two first terms.

Due to aforementioned behavior of s-wave spin-quartet nd elastic scattering, we use larger harmonic oscillator trap lengths up to $b_{HO} \leqslant 140$ fm which allows us to extract $n - d$ $S = 3/2$ scattering phase shifts at very low relative momenta down to $k^2 \approx 0.0002$ fm^{-2}. The LO and NLO scattering lengths $a_{nd}^{3/2}$ and effective ranges $r_{nd}^{3/2}$ are then obtained fitting ERE, Eq. (11), to $k \cot \delta_{nd}^{3/2}$ values for $k^2 \in [0.0002, 0.002]$ fm^{-2}. In Figs. 5(a) and 5(b) we present the corresponding values as a function of momentum cutoff λ. Considering again residual cutoff variation and numerical accuracy of our predictions we get

$$\text{LO}: \ a_{nd}^{3/2} = 6.355(25) \text{ fm}, \quad r_{nd}^{3/2} = 1.71(85) \text{ fm},$$
$$\text{NLO}: \ a_{nd}^{3/2} = 6.322(5) \text{ fm}, \quad r_{nd}^{3/2} = 1.875(65) \text{ fm}.$$

The red dotted lines in Figs. 5(a) and 5(b) show zero-range LO nd spin-quartet scattering length and effective range calculated using the STM. Apparently, our LO results converge to these values. Extrapolating $[f(\lambda) = f(\infty) + \alpha/\lambda]$ LO results for $\lambda \geqslant 7$ fm^{-1} yields $a_{nd}^{3/2}(\infty)/a_{NN}^1 = 1.17906(3)$ and $r_{nd}^{3/2}(\infty)/a_{NN}^1 = -0.037(3)$ values which agree with the STM prediction $a_{nd}^{3/2}(\text{STM})/a_{NN}^1 = 1.179066$ and $r_{nd}^{3/2}(\text{STM})/a_{NN}^1 = -0.0383$.

Our NLO results are compared to predictions of universal relations for the fermionic atom-dimer scattering length a_{a-dm} and effective range r_{a-dm} given, up to linear correction in atom-atom effective range, by the atom-atom scattering pa-

rameters a_{aa} and r_{aa} [12–14,52],

$$\frac{a_{a-dm}}{a_{aa}} = 1.179066 - 0.03595 \frac{r_{aa}}{a_{aa}}, \tag{15}$$

$$\frac{r_{a-dm}}{a_{aa}} = -0.0383 + 1.0558 \frac{r_{aa}}{a_{aa}}. \tag{16}$$

Using the NN spin-triplet scattering parameters this corresponds to $a_{nd}^{3/2}/a_{NN}^1 = 1.16743$ and $r_{nd}^{3/2}/a_{NN}^1 = 0.30324$. As in the LO case we extrapolate our NLO results to the zero-range limit obtaining $a_{nd}^{3/2}(\infty)/a_{NN}^1 = 1.1666(8)$ and $r_{nd}^{3/2}(\infty)/a_{NN}^1 = 0.32(2)$ values which agree with the predictions of Eqs. (15) and (16).

We would like to mention that not considering large enough b_{HO} in our LO calculations one can obtain phase shifts in the momentum region $k^2 \geqslant 0.02$ fm^{-2}, where the corresponding $k \cot \delta_{nd}^{3/2}$ behavior might seem linear as a function of k^2. This can be misinterpreted in terms of larger LO $r_{nd}^{3/2}$ effective range contradicting the STM result. In fact, performing $\lambda \to \infty$ extrapolation of these "wrong" $r_{nd}^{3/2}$ values leads to $r_{nd}^{3/2}(\infty)/a_{NN}^1 = 0.082(2)$, in agreement with result $r_{nd}^{3/2}(\infty)/a_{NN}^1 = 0.08(1)$ of Ref. [53], where HO trap was applied as well.

3. Zero-momentum nd scattering

So far our predictions of the s-wave nd elastic scattering have been compared to scarce experimental results of Ref. [26]. In order to access experimental information for zero-momentum, $a_{nd}^{1/2}$ and $a_{nd}^{3/2}$ in particular, several experiments were performed which provide certain constraints on the possible scattering length values $(a_{nd}^{1/2}; a_{nd}^{3/2})$.

In Fig. 6 we show the $(a_{nd}^{1/2}; a_{nd}^{3/2})$ plane with the experimental constraints imposed by the following measurements: size of $a_{nd}^{1/2}$ and $a_{nd}^{3/2}$ (grey) [54], $a_{nd}^{1/2}/a_{nd}^{3/2}$ ratio (yellow) [55], experimental value of nd zero-momentum total cross
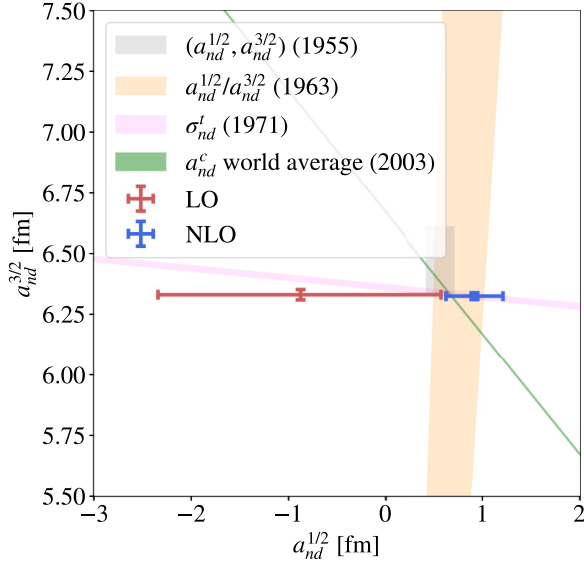
FIG. 6. The $(a_{nd}^{1/2}; a_{nd}^{3/2})$ plane with experimental constraints imposed by different measurements—size of $a_{nd}^{1/2}$ and $a_{nd}^{3/2}$ (grey) [54], $a_{nd}^{1/2}/a_{nd}^{3/2}$ ratio (yellow) [55], nd zero-momentum total cross-section (pink) [25], and world average of experimental coherent scattering length (green) [56]. Our $\not\pi$EFT LO and NLO predictions are shown by red and blue error bars, respectively.

section (pink) [25]

$$\sigma_{nd}^t = 4\pi \left[\frac{1}{3} \left(a_{nd}^{1/2}\right)^2 + \frac{2}{3} \left(a_{nd}^{3/2}\right)^2 \right], \qquad (17)$$

and the world average of experimental nd coherent scattering length (green) [56]

$$a_{nd}^c = \frac{1}{3} a_{nd}^{1/2} + \frac{2}{3} a_{nd}^{3/2}. \qquad (18)$$

Our LO and NLO predictions of $(a_{nd}^{1/2}; a_{nd}^{3/2})$ scattering lengths are shown using red and blue error bars, respectively. Corresponding uncertainties are induced by numerics and residual $\lambda \in [1.25, 10] \, \text{fm}^{-1}$ dependence of our results.

Our nd scattering length predictions can be further compared to the values extracted from experimental data. The modified ERE, Eq. (14), was used to fit experimental spin-doublet nd phase shifts extracting scattering length $a_{nd}^{1/2} = 0.29 \, \text{fm}$ [26]. Somewhat larger experimental scattering length $a_{nd}^{1/2} = 0.65(4) \, \text{fm}$ was extracted from zero-energy scattering measurements together with its spin-quartet equivalent $a_{nd}^{3/2} = 6.35(2) \, \text{fm}$ [25]. Using a compilation of $a_{nd}^{3/2}$ theoretical predictions a more precise $a_{nd}^{1/2} = 0.645 \pm 0.003(\text{exp}) \pm 0.007(\text{theory}) \, \text{fm}$ value was obtained from the world average coherent scattering length [56].

C. Four nucleons

A system of four nucleons might exist in nine different spin-isospin channels where both the total spin S and the total isospin I can get any value from 0, 1, and 2. Among these channels only $S, I = (0, 0)$ allows all four nucleons to occupy the s shell and it is solely this channel that contributes, within our framework, to the ^{4}He(0^+) ground state. As shown
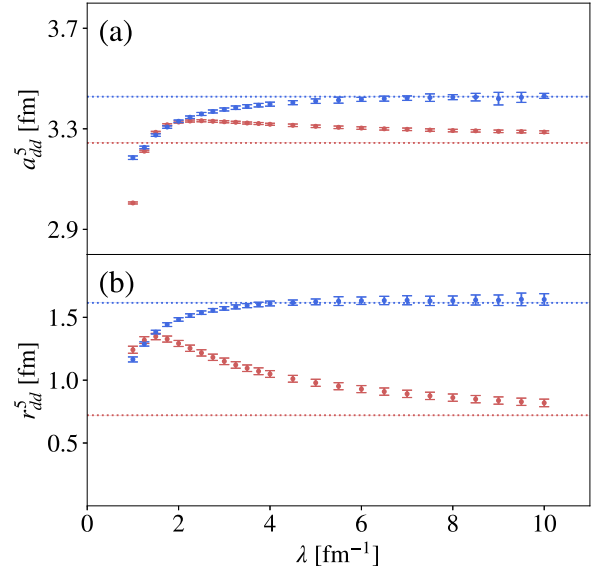

FIG. 7. The dd scattering length a_{dd}^5 (a) and effective range r_{dd}^5 (b) in spin-isospin $S, I = (2, 0)$ four-body channel at LO (red) and NLO (blue) as a function of the momentum cutoff λ. Error bars denote the numerical uncertainty of our results. Red and blue dotted lines mark predicted dimer-dimer scattering parameters using Eq. (19) for $a_{aa}, r_{aa} = (5.419, 0)$ fm and $a_{aa}, r_{aa} = (5.419, 1.753)$ fm, respectively.

earlier, the inclusion of two- and three-body NLO corrections to B_4 leads to results outside of validity of perturbation theory and which deviate from the experimental value. Following Ref. [6], we assume that NLO cutoff invariance in a nuclear case might be recovered by a perturbative inclusion of a four-body force. However, it is not clear whether the remaining S, I four-body channels are affected as well or the necessity of four-body force remains pertinent only to the $S, I = (0, 0)$ channel with none of the nucleons being Pauli blocked.

In order to explore cutoff dependence we study s-wave elastic $3 + 1$ scattering in $S, I = (0, 0)$, (1,0), (0,1), and (1,1) four-body channels and $2 + 2$ scattering in $S, I = (2, 0)$ four-body channel at LO and NLO $\not\pi$EFT. Here, $2N$ and $3N$ stand for the deuteron and triton ground state, respectively. Remaining channels $S, T = (0, 2)$, (1,2), (2,1), and (2,2) are not considered in this work since they do not support partition into two subclusters.

1. S=2 channel

The $S, I = (2, 0)$ channel allows four-body partition into two deuteron bound states. Here, we disregard Coulomb interaction, consequently, we do not compare our results of $S = 2$ s-wave ($^5S_2$) dd elastic scattering to Refs. [57,58] where Coulomb force enters strongly at low momenta. Instead, similarly as for $S = 3/2$ nd scattering, at LO and NLO $\not\pi$EFT only s-wave NN spin-triplet interaction contributes and our calculations can be analyzed through universality in fermionic dimer-dimer scattering. The corresponding fermionic dimer-dimer scattering length a_{dm-dm} and effective range r_{dm-dm} can be parametrized through the atom-atom scattering parameters
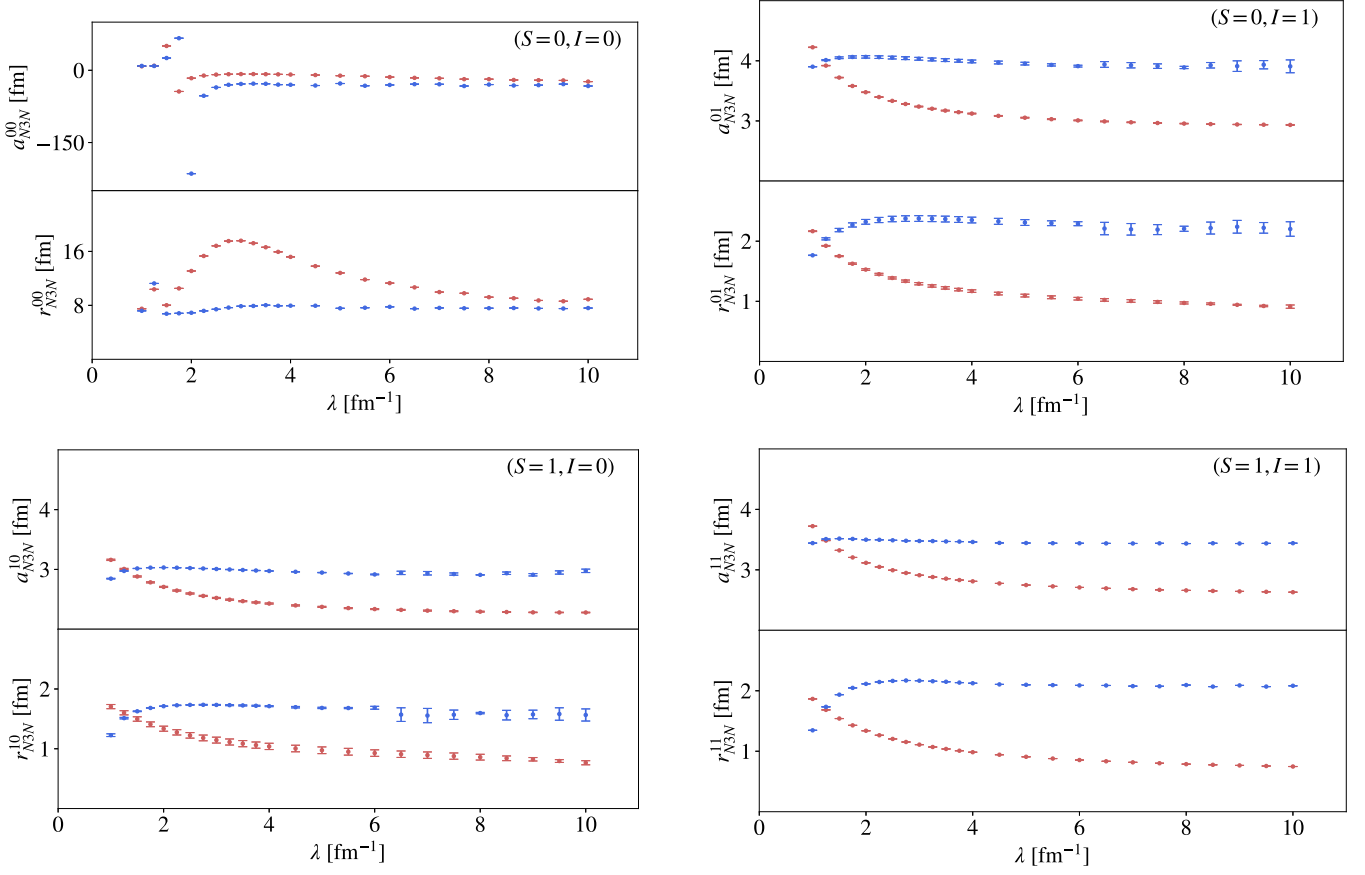
FIG. 8. $N3N$ scattering lengths a_{N3N}^{SI} and effective ranges r_{N3N}^{SI} at LO (red) and NLO (blue), as a function of increasing momentum cutoff λ. Scattering parameters are shown for $S, I = (0, 1)$, $(1,1)$, $(1,0)$, and $(0,0)$ spin-isospin four-body channels. Error bars denote the numerical uncertainty of our results.

a_{aa} and r_{aa} by [15,59]

$$\frac{a_{dm-dm}}{a_{aa}} = 0.5986 + 0.105\frac{r_{aa}}{a_{aa}} \pm 0.0005;$$

$$\frac{r_{dm-dm}}{a_{aa}} = 0.133 + 0.51\frac{r_{aa}}{a_{aa}} \pm 0.002. \quad (19)$$

Here, we repeat the procedure already used to analyze spin-quartet $S = 3/2$ nd scattering. For LO (zero range) NN spin-triplet scattering parameters Eq. (19) yields $a_{dm-dm} = 3.2438(5)$ fm and $r_{dm-dm} = 0.721(2)$ fm and for the NLO case $a_{dm-dm} = 3.4278(5)$ fm and $r_{dm-dm} = 1.615(2)$ fm. If $^5S_2$ dd elastic scattering exists in a universality window, i.e., range of validity of Eq. (19), we expect that calculated LO and NLO deuteron-deuteron scattering parameters should converge for $\lambda \to \infty$ to these values of a_{dm-dm} and r_{dm-dm}.

We calculate dd phase shifts in the $^5S_2$ channel at LO and NLO $\not\pi$EFT. Corresponding scattering lengths a_{dd} and effective ranges r_{dd} are shown as a function of $\lambda \in [1, 10]$ fm^{-1} in Figs. 7(a) and 7(b), respectively. We observe that both LO and NLO predictions converge with increasing λ to a_{dm-dm} and r_{dm-dm} values predicted via Eq. (19). Our calculations thus demonstrate that within $\not\pi$EFT, elastic dd scattering in the $^5S_2$ channel is in line with the universal prediction of fermionic dimer-dimer scattering of Refs. [15,59], moreover,

our NLO results show no requirement of four-body force in this channel.

2. S=0 and S=1 channel

Moving to $3 + 1$ scattering, we first check cutoff dependence in $S, I = (0, 0)$, $(1,0)$, $(0,1)$, and $(1,1)$ four-body channels. In Fig. 8 we show the scattering lengths and effective ranges extracted from the calculated s-wave $N - 3N$ phase shifts. We find that in $S, I = (1, 0)$, $(0,1)$, and $(1,1)$ four-body channels there is no requirement of additional four-body force. In the $S, I = (0, 0)$ channel the four-body force, Eq. (7), is included and, as can be seen from the upper left panel of Fig 8, our NLO results indeed converge with λ. The behavior of a_{NN}^{00} and r_{NN}^{00} scattering parameters at small $\lambda < 2$ fm^{-1} can be attributed to the passing of the first 0^+ excited state of ^{4}He from the bound state region to the continuum.

With no Coulomb interaction, our $N - 3N$ results in Fig. 8 might be regarded as nt or n^3He scattering. Adopting full isospin symmetry the nt system might scatter either in the $S, I = (0, 1)$ (spin-singlet) or $S, I = (1, 1)$ (spin-triplet) four-body channel. For n^3He, the corresponding s-wave spin-singlet and spin-triplet scattering has contribution from two four-body spin-isospin channels $S, I = (0, 1) + (0, 0)$ and $S, I = (1, 1) + (1, 0)$, respectively. To the best of our
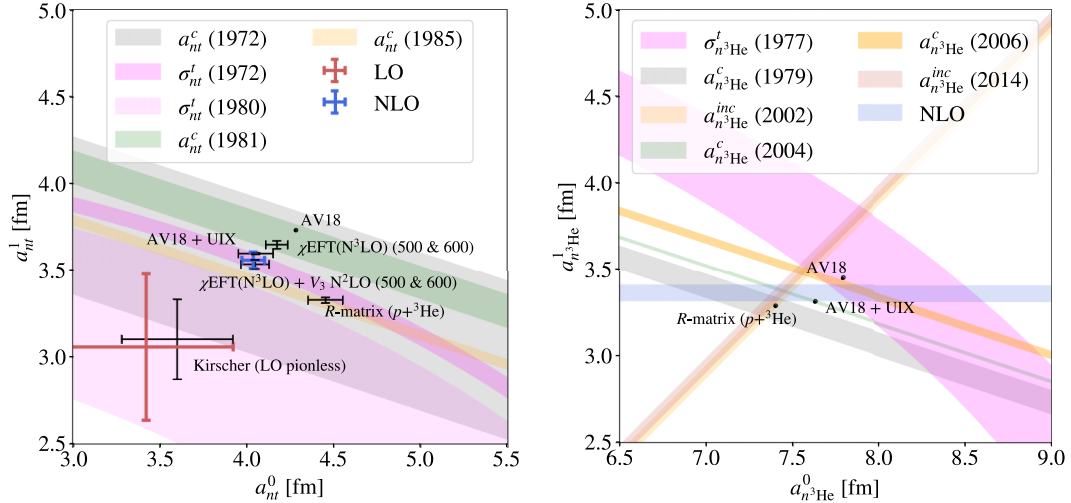
FIG. 9. Left panel: The $(a_{nt}^0; a_{nt}^1)$ plane with experimental constraints imposed by different measurements—size of coherent scattering length a_{nt}^c (1972) [60], (1981) [61], (1985) [62], and total cross section at zero momentum σ_{nt}^t (1972) [60], σ_{nt}^t (1980) [63]. Our $\cancel{\pi}$EFT LO and NLO predictions are shown by red and blue error bars, respectively. Right panel: The $(a_{n^3\mathrm{He}}^0; a_{n^3\mathrm{He}}^1)$ plane with experimental constraints imposed by different measurements—size of coherent scattering length $a_{n^3\mathrm{He}}^c$ (1979) [68], (2004) [69], (2006) [70]; size of incoherent scattering length $a_{n^3\mathrm{He}}^{\mathrm{inc}}$ (2002) [71], (2014) [72]; and total cross section at zero momentum $\sigma_{n^3\mathrm{He}}^t$ (1977) [73]. Our $a_{n^3\mathrm{He}}^1$ NLO prediction is represented by a blue band. For references to individual theoretical predictions in both panels (black dots/error bars) see the text.

knowledge, there are no available s-wave low momentum experimental phase shifts below the $t/^3$He breakup threshold. Consequently, only the zero momentum part of our results, in terms of scattering lengths, will be compared to a collection of available experimental data and theoretical works.

3. Zero momentum nt and n³He scattering

Unlike in the nd case, more unsettled situation persists in zero-momentum nt and n^3He scattering. Here, spin-singlet (a_{N3N}^0) and spin-triplet (a_{N3N}^1) scattering lengths, $N3N \in \{nt, n^3\mathrm{He}\}$, are constrained by experimentally measured coherent scattering length

$$a_{N3N}^c = \tfrac{1}{4}a_{N3N}^0 + \tfrac{3}{4}a_{N3N}^1, \qquad (20)$$

incoherent scattering length

$$a_{N3N}^{\mathrm{inc}} = \frac{\sqrt{3}}{4}\left[a_{N3N}^1 - a_{N3N}^0\right], \qquad (21)$$

or the total cross section at zero momentum

$$\sigma_{N3N}^t = 4\pi\left[\tfrac{1}{4}\left(a_{N3N}^0\right)^2 + \tfrac{3}{4}\left(a_{N3N}^1\right)^2\right]. \qquad (22)$$

In the left panel of Fig. 9 we show the $(a_{nt}^0; a_{nt}^1)$ plane with shaded areas representing possible sets of scattering length values suggested by experimentally measured a_{nt}^c [60–62] or σ_{nt}^t [60,63]. As can be seen from the figure, experimental results are mostly in mutual disagreement or burdened by a rather large experimental uncertainty. Adding to the figure also theoretical predictions of microscopic four-body calculations using AV18 NN interaction with and without Urbana IX three-body force [64,65], and χEFT(N^{3}LO) NN interaction with and without three-body χEFT(N^{2}LO) force [66] suggests smaller area of possible $(a_{n^3\mathrm{H}}^0; a_{n^3\mathrm{H}}^1)$. Interestingly, scattering lengths extracted from the R-matrix analysis

of p^3He scattering data [67] seem to be slightly shifted from these theoretical results. At LO $\cancel{\pi}$EFT the size of a_{nt}^0 and a_{nt}^1 scattering lengths was predicted in Ref. [33], here, a rather large theoretical uncertainty was assigned via momentum cutoff variation between 2 and 8 fm^{-1}. In the same work, the author numerically demonstrated a correlation between the triton binding energy B_3 and $(a_{nt}^0, a_{n^3\mathrm{H}}^1)$ where with decreasing B_3 the magnitude of scattering lengths grows. This is in agreement with slightly shifted AV18 and chiral results with no three-body force—disregarding the three-body interaction in these calculations slightly underestimates experimental B_3.

We extract nt s-wave scattering parameters in spin-singlet and spin-triplet from our $N - 3N$ calculations in $S, I = (0, 1)$ and $S, I = (1, 1)$ four-body channels, respectively. Note that within our approach B_3 is used to renormalize a three-body contact interaction, consequently, $S, I = (1/2, 1/2)$ three-body bound state $(3N)$ is kept consistently fixed at triton experimental binding energy both at LO and NLO. Taking into account numerical errors and residual cutoff variation for $\lambda \in [1.25, 10]$ fm^{-1} we obtain scattering length values

$$\mathrm{LO} \ : \ a_{nt}^0 = 3.42(50) \ \mathrm{fm}, \quad a_{nt}^1 = 3.06(42) \ \mathrm{fm},$$

$$\mathrm{NLO} \ : \ a_{nt}^0 = 4.035(65) \ \mathrm{fm}, \quad a_{nt}^1 = 3.566(47) \ \mathrm{fm},$$

which are displayed by red (LO) and blue (NLO) error bars in the left panel of Fig. 9. Our LO predictions are in agreement with Ref. [33]. A slightly larger uncertainty of our LO results is induced by a larger λ interval considered for theoretical error assessment than in Ref. [33]. This error estimate is significantly reduced including subleading effective range corrections. At NLO resulting a_{nt}^0 and a_{nt}^1 are predicted in remarkable agreement with AV18 and χEFT microscopic results with three-body forces included.

In the right panel of Fig. 9 we depict the $(a_{n^3\mathrm{He}}^0; a_{n^3\mathrm{He}}^1)$ plane where shaded areas denote possible sets of scattering

length values suggested by experimental $a_{n^3\text{He}}^c$ [68–70], $a_{n^3\text{He}}^{\text{inc}}$ [71,72], and $\sigma_{n^3\text{He}}^t$ [73]. Similarly as in the n^3H case some experimental constraints are in mutual disagreement. There are only few available theoretical results—microscopic calculation using AV18 interaction with and without Urbana IX three-body force and R-matrix analysis of p^3He scattering data [74].

In our $\pi\!\!\!/$EFT calculations of n^3He scattering we fix at NLO the ground state energy of the $S, I = (1/2, 1/2)$ three-body system at experimental $B(^3\text{He}) = 7.718$ MeV [48], hence we simulate the correct position of the corresponding $3 + 1$ threshold. The spin-triplet scattering length is then calculated by isospin-averaging $a_{n^3\text{He}}^1 = \sqrt{1/2(a_{N3N}^{(1,0)})^2 + 1/2(a_{N3N}^{(1,1)})^2}$ over $S, I = (1, 0)$ and $(1,1)$ four-body channels,

$$\text{NLO}: \quad a_{n^3\text{He}}^1 = 3.360(45) \text{ fm,}$$

where the error is estimated in the same manner as in the case of nt scattering. Our result is then depicted in the right panel of Fig. 9 in a form of a blue horizontal band showing consistency with the previous theoretical studies.

Not considering the Coulomb interaction introduces certain shortcomings into our description of spin-singlet n^3He scattering. First, t and ^{3}He ground state energies are degenerate, which leads to degenerate pt and n^3He thresholds as well. As a result, the position of the 0_2^+ resonance in ^{4}He is not correctly reproduced. The same subsequently holds for the low-energy n^3He scattering in the $S, I = (0, 0)$ four-body channel which is strongly affected by the resonance position. Therefore, we give here only our result for the isospin-triplet $S, I = (0, 1)$ component of the $a_{n^3\text{He}}^0$ scattering length

$$\text{NLO}: \quad a_{n^3\text{He}}^{(0,1)} = 4.171(82) \text{ fm,} \tag{23}$$

keeping in mind that its dominant $I = 0$ contribution has to be determined in future studies with Coulomb interaction included.

VI. CONCLUSION

We performed a thorough analysis of s-wave scattering processes in $A \leqslant 4$ nuclear systems within the first two orders of $\pi\!\!\!/$EFT. Using the stochastic variational method we solved the few-body Schrödinger equation for nuclear bound states both inside and outside the shallow harmonic oscillator trap. This allowed us to extract s-wave scattering phase shifts using the Busch formula in all possible A-body spin-isospin channels which support partition into two subclusters.

Our EFT was fitted to six well-established experimental parameters. At LO we fixed the two-body LECs using the experimental nn spin-singlet and np spin-triplet scattering lengths. The three-body LEC was fitted to the triton ground state binding energy. NLO terms were included perturbatively. At this order, LECs of two-body momentum-dependent interaction were constrained by the experimental effective ranges in nn spin-singlet and np spin-triplet channels. In agreement with the results of Ref. [6], we found it necessary to include at NLO a four-body force to retain cutoff invariant predictions

once all four nucleons are allowed to occupy the s shell, i.e., in the $S, I = (0, 0)$ four-body channel. We thus have to include one four-body LEC, which is fitted to the 0^+ ground state binding energy of ^{4}He.

Using this theory, we calculated elastic nd, dd, nt, and n^3He s-wave scattering at LO and NLO $\pi\!\!\!/$EFT. For a wide momentum cutoff interval $\lambda \in [1, 10] \text{ fm}^{-1}$ we numerically demonstrated that all our predictions converge with increasing cutoff once $\lambda \gg m_\pi$, i.e., when the momentum cutoff is much larger than the breakup scale of the theory. Our results further show that no NLO four-body force is needed in the $S, I = (0, 1)$, $(1,0)$, $(1,1)$, and $(2,0)$ spin-isospin four-body channels, while its inclusion in $S, I = (0, 0)$ provides cutoff invariant scattering predictions. The remaining $S, I = (0, 2)$, $(1,2)$, $(2,2)$, and $(2,1)$ four-body channels were not studied; however, it is reasonable to assume that since in these channels at least two nucleons are Pauli blocked from the s shell no four-body force will be needed as well.

Despite the simplicity of the $\pi\!\!\!/$EFT approach, all our NLO low energy scattering predictions are in remarkable agreement with the available experimental data or results of other interaction models. In particular, predicted nt scattering lengths values basically coincide with results obtained with the AV18+UIX potential [64,65] or χEFT(N ^{3}LO) interaction with N ^{2}LO three-body force [66]. For clarity we summarize our nd, nt, and n^3He scattering length and effective range predictions together with a calculated energy of the nd $S = 1/2, I = 1/2$ virtual state, and compare with the available theoretical and experimental results in Table I.

The apparent shortcoming of our study is a lack of Coulomb interaction. Its inclusion would allow us to compare our predictions with more extensive pd, dd, p^3H, or p^3He scattering data. The Coulomb interaction is, in particular, important for a correct description of the p^3H and n^3He threshold and the position of a narrow 0_2^+ resonance in ^{4}He. In future work it would be interesting to study Coulomb inclusion alongside NLO corrections in $A \geqslant 4$ systems which, to the best of our knowledge, have not been performed so far.

Our $\pi\!\!\!/$EFT calculations should be regarded as a stepping stone towards a study of subleading corrections in heavier nuclear systems beyond the s shell. While this work is the first of its kind where effective range corrections are introduced perturbatively in a four-body nuclear system, $A \geqslant 5$ nuclear systems remain unexplored. One of the main advantages of the Hamiltonian formalism, adopted in our calculations, is a rather straightforward extension to p-wave scattering such as n^3H or n^4He, strongly affected by the position of ^{4}H and ^{5}He resonances, or even to heavier nuclei. So far it has been concluded that at LO nuclear systems beyond the s shell do not retain bound states in the zero-range contact limit; instead, they break into bound s-shell subclusters [78,79]. However, as argued in Ref. [79], including subleading corrections might change the outcome of LO calculations and bring these systems to the bound state region. It would be interesting to explore to which extent this might be done considering NLO terms.

The form of effective range corrections, methods, and procedures outlined in this work are applicable beyond the

TABLE I. Theoretical and experimental nd, nt, and n^3He scattering length and effective range values in fm together with energies of nd $S = 1/2$, $I = 1/2$ virtual state $E_{nd}^{1/2}$ in MeV. We note that in some $\cancel{\pi}$EFT works [16,18,19,22–24] three-body LEC(s) are fitted to reproduce experimental scattering length $a_{nd}^{1/2} = 0.65(4)$ fm [25].

Scattering	Values		Exp/Model
nd	$a_{nd}^{1/2}$	$a_{nd}^{3/2}$	
	0.29	5.6	exp (nd phase shifts) [26]
	0.65(4)	6.35(2)	exp (extracted from σ_{nd}^t and a_{nd}^c) [25]
	0.645(3)(7)	—	exp a_{nd}^c + collection of theor. $a_{nd}^{3/2}$ results [56]
	1.304	6.346	AV18 [75]
	0.636	6.437	AV18 + UIX [75]
	—	6.33(10)	$\cancel{\pi}$EFT (NLO); nonperturbative [7]
	—	6.7(7)	$\cancel{\pi}$EFT (NLO); nonperturbative [17]
	—	6.354(20)	$\cancel{\pi}$EFT (N^{2}LO); partial resummation [20]
	—	6.19(30)	$\cancel{\pi}$EFT (N^{2}LO); perturbative [21]
	0.92(29)	6.322(5)	This work $\cancel{\pi}$EFT (NLO); perturbative
	$r_{nd}^{1/2}$	$r_{nd}^{3/2}$	
	1.7	—	exp (nd phase shifts) [26]
	—	1.8(1)	$\cancel{\pi}$EFT (N^{2}LO); partial resummation [20]
	1.74(33)	1.875(65)	This work $\cancel{\pi}$EFT (NLO); perturbative
	$E_{nd}^{1/2}$ (virt.)		
	−0.48		separable potential [51]
	−0.574		$\cancel{\pi}$EFT (LO) [24]
	−0.503(31)		This work $\cancel{\pi}$EFT (NLO); perturbative
nt	a_{nt}^0	a_{nt}^1	
	3.60(32)	3.10(23)	$\cancel{\pi}$EFT (LO) [33]
	4.453	3.325	R-matrix ($p + {}^3$He) [67]
	4.28	3.73	AV18 [64]
	4.05(10)	3.595(5)	AV18 + UIX [64,65]
	4.171(63)	3.646(23)	χEFT(N^{3}LO) (500 & 600) [66]
	4.046(81)	3.533(26)	χEFT(N^{3}LO) + V_3 N^{2}LO (500 & 600) [66]
	4.035(65)	3.566(47)	This work $\cancel{\pi}$EFT (NLO); perturbative
	r_{nt}^0	r_{nt}^1	
	2.08	1.72	AV18 + UIX [76]
	2.117(10)	1.743(10)	χEFT(N^{3}LO) (500 & 600) [77]
	2.058(4)	1.709(6)	χEFT(N^{3}LO) + V_3 N^{2}LO (500 & 600) [77]
	2.17(15)	1.76(41)	This work $\cancel{\pi}$EFT (NLO); perturbative
n^3He	$a_{n^3\text{He}}^0$	$a_{n^3\text{He}}^1$	
	7.790	3.448	AV18 [74]
	7.629	3.311	AV18 + UIX [74]
	6.98	3.20	R-matrix ($p + {}^3$He) [74]
	7.5(6)	—	$\cancel{\pi}$EFT (NLO); nonperturbative [34]
	—	3.360(45)	This work $\cancel{\pi}$EFT (NLO); perturbative
	$r_{n^3\text{He}}^0$	$r_{n^3\text{He}}^1$	
	—	1.83(28)	This work $\cancel{\pi}$EFT (NLO); perturbative

scope of nuclear systems. In fact, they might be used in an analysis of LQCD data [80–83] or even in a study of more exotic systems such as hypernuclei [84–87], and mesic nuclei [88]. As might be seen in our work, including NLO terms dramatically improves the predictive power of the theory and the same outcome might be expected in these systems as well.

[1] H.-W. Hammer, S. König, and U. van Kolck, Nuclear effective field theory: Status and perspectives, Rev. Mod. Phys. **92**, 025004 (2020).

[2] E. P. Wigner, Lower limit for the energy derivative of the scattering phase shift, Phys. Rev. **98**, 145 (1955).

[3] L. H. Thomas, The interaction between a neutron and a proton and the structure of ^{3}H, Phys. Rev. **47**, 903 (1935).

[4] P. F. Bedaque, H.-W. Hammer, and U. van Kolck, Renormalization of the Three-Body System with Short-Range Interactions, Phys. Rev. Lett. **82**, 463 (1999); The three boson system with short-range interactions, Nucl. Phys. A **646**, 444 (1999); Effective theory of the triton, **676**, 357 (2000).

[5] V. Efimov, Energy levels arising from resonant two-body forces in a three-body system, Phys. Lett. B **33**, 563 (1970).

[6] B. Bazak, J. Kirscher, S. König, M. Pavón Valderrama, N. Barnea, and U. van Kolck, Four-Body Scale in Universal Few-Boson Systems, Phys. Rev. Lett. **122**, 143001 (2019).

[7] P. F. Bedaque and U. van Kolck, Nucleon-deuteron scattering from an effective field theory, Phys. Lett. B **428**, 221 (1998).

[8] P. F. Bedaque, H.-W. Hammer, and U. van Kolck, Effective theory for neutron-deuteron scattering: Energy dependence, Phys. Rev. C **58**, R641(R) (1998).

[9] V. Efimov, Energy levels of three resonantly interacting particles, Nucl. Phys. A **210**, 157 (1973).

[10] Y. Castin, C. Mora, and L. Pricoupenko, Four-Body Efimov Effect for Three Fermions and a Lighter Particle, Phys. Rev. Lett. **105**, 223201 (2010).

[11] B. Bazak and D. S. Petrov, Five-Body Efimov Effect and Universal Pentamer in Fermionic Mixtures, Phys. Rev. Lett. **118**, 083002 (2017).

[12] G. V. Skorniakov and K. A. Ter-Martirosian, Three body problem for short range forces. I. Scattering of low energy neutrons by deuterons, Zh. Eksp. Teor. Fiz. **31**, 775 (1956) [Sov. Phys. JETP **4**, 648 (1957)].

[13] B. E. Grinyuk, I. V. Simenog, and A. I. Sitnichenko, Model-independent description of quartet *nd* scattering at low energies, Yad. Fiz. **39**, 402 (1984) [Sov. J. Nucl. Phys. **39**, 253 (1984)].

[14] D. S. Petrov, Three-body problem in Fermi gases with short-range interparticle interaction, Phys. Rev. A **67**, 010703(R) (2003).

[15] D. S. Petrov, C. Salomon, and G. V. Shlyapnikov, Weakly Bound Dimers of Fermionic Atoms, Phys. Rev. Lett. **93**, 090404 (2004).

[16] F. Gabbiani, P. F. Bedaque, and H. W. Grießhammer, Higher partial waves in an effective field theory approach to scattering, Nucl. Phys. A **675**, 601 (2000).

[17] P. F. Bedaque and H. W. Grießhammer, Quartet S wave neutron deuteron scattering in effective field theory, Nucl. Phys. A **671**, 357 (2000).

[18] H.-W. Hammer and T. Mehen, Range corrections to doublet S-wave neutron-deuteron scattering, Phys. Lett. B **516**, 353 (2001).

[19] P. F. Bedaque, G. Rupak, H. W. Grießhammer, and H.-W. Hammer, Low energy expansion in the three body system to all orders and the triton channel, Nucl. Phys. A **714**, 589 (2003).

[20] H. W. Grießhammer, Improved convergence in the three-nucleon system at very low energies, Nucl. Phys. A **744**, 192 (2004).

[21] J. Vanasse, Fully perturbative calculation of nd scattering to next-to-next-to-leading order, Phys. Rev. C **88**, 044001 (2013).

[22] A. Margaryan, R. P. Springer, and J. Vanasse, nd scattering and the A_y puzzle to next-to-next-to-next-to-leading order, Phys. Rev. C **93**, 054001 (2016).

[23] S. König, Second-order perturbation theory for ^{3}He and pd scattering in pionless EFT, J. Phys. G: Nucl. Part. Phys. **44**, 064007 (2017).

[24] G. Rupak, A. Vaghani, R. Higa, and U. van Kolck, Fate of the neutron-deuteron virtual state as an Efimov level, Phys. Lett. B **791**, 414 (2019).

[25] W. Dilg, L. Koester, and W. Nistler, The neutron-deuteron scattering lengths, Phys. Lett. B **36**, 208 (1971).

[26] W. T. H. van Oers and J. D. Seagrave, The neutron-deuteron scattering lengths, Phys. Lett. B **24**, 562 (1967).

[27] A. C. Phillips and G. Barton, Relations between low energy three-nucleon observables, Phys. Lett. B **28**, 378 (1969).

[28] C. Ji, D. R. Phillips, and L. Platter, The three-boson system at next-to-leading order in an effective field theory for systems with a large scattering length, Ann. Phys. (NY) **327**, 1803 (2012).

[29] C. Ji and D. R. Phillips, Effective field theory analysis of three-boson systems at next-to-next-to-leading order, Few-Body Syst. **54**, 2317 (2013).

[30] S. König and H.-W. Hammer, Precision calculation of the quartet-channel p-d scattering length, Phys. Rev. C **90**, 034005 (2014).

[31] J. Vanasse, D. A. Egolf, J. Kerin, S. König, and R. P. Springer, ^{3}He and pd scattering to next-to-leading order in pionless effective field theory, Phys. Rev. C **89**, 064003 (2014).

[32] S. König, H. W. Grießhammer, and H.-W. Hammer, The proton-deuteron system in pionless EFT revisited, J. Phys. G: Nucl. Part. Phys. **42**, 045101 (2015).

[33] J. Kirscher, Zero-energy neutron-triton and proton-Helium-3 scattering with $\not\pi$EFT, Phys. Lett. B **721**, 335 (2013).

[34] J. Kirscher, H. W. Grießhammer, D. Shukla, and H. M. Hofmann, Universal correlations in pion-less EFT with the resonating group method: Three and four nucleons, Eur. Phys. J. A **44**, 239 (2010).

[35] T. Busch, B. G. Englert, K. Rzazewski, and M. Wilkens, Two cold atoms in a harmonic trap, Found. Phys. **28**, 549 (1998).

[36] A. Suzuki, Y. Liang, and R. K. Bhaduri, Two-atom energy spectrum in a harmonic trap near a Feshbach resonance at higher partial waves, Phys. Rev. A **80**, 033601 (2009).

[37] Y. Suzuki and K. Varga, *Stochastic Variational Approach to Quantum-Mechanical Few-Body Problems* (Springer, Berlin, 1998).

[38] S. R. Beane, T. D. Cohen, and D. R. Phillips, The potential of effective field theory in NN scattering, Nucl. Phys. A **632**, 445 (1998).

[39] M. Lüscher, Volume dependence of the energy spectrum in massive quantum field theories. II. Scattering states, Commun. Math. Phys. **105**, 153 (1986); Two-particle states on a torus and their relation to the scattering matrix, Nucl. Phys. B **354**, 531 (1991).

[40] I. Stetcu, J. Rotureau, B. R. Barrett, and U. van Kolck, An effective field theory approach to two trapped particles, Ann. Phys. (NY) **325**, 1644 (2010).

[41] J. Rotureau, I. Stetcu, B. R. Barrett, and U. van Kolck, Two and three nucleons in a trap, and the continuum limit, Phys. Rev. C **85**, 034003 (2012).

[42] M. Schäfer, B. Bazak, N. Barnea, and J. Mareš, Nature of the $\Lambda nn(J^\pi = 1/2^+, I = 1)$ and $^3_\Lambda$H*$(J^\pi = 3/2^+, I = 0)$ states, Phys. Rev. C **103**, 025204 (2021).

[43] D. E. González Trotter *et al.*, Neutron-deuteron breakup experiment at $E_n = 13$ MeV: Determination of the $^1S_0$ neutron-neutron scattering length a_{nn}, Phys. Rev. C **73**, 034001 (2006).

[44] Q. Chen *et al.*, Measurement of the neutron-neutron scattering length using the $\pi^- d$ capture reaction, Phys. Rev. C **77**, 054002 (2008).

[45] R. Machleidt, High-precision, charge-dependent Bonn nucleon-nucleon potential, Phys. Rev. C **63**, 024001 (2001).

[46] H. Ouerdane, M. J. Jamieson, D. Vrinceanu, and M. J. Cavagnero, The variable phase method used to calculate and correct scattering lengths, J. Phys. B: At. Mol. Opt. Phys. **36**, 4055 (2003).

[47] G. A. Miller, B. M. K. Nefkens, and I. Šlaus, Charge symmetry, quarks and mesons, Phys. Rep. **194**, 1 (1990).

[48] J. E. Purcell, J. H. Kelley, E. Kwan, C. G. Sheu, and H. R. Weller, Energy levels of light nuclei $A = 3$, Nucl. Phys. A **848**, 1 (2010).

[49] D. R. Tilley, H. R. Weller, and G. M. Hale, Energy levels of light nuclei $A = 4$, Nucl. Phys. A **541**, 1 (1992).

[50] H. W. Grießhammer, A consistency test of EFT power countings from residual cutoff dependence, Eur. Phys. J. A **56**, 118 (2020).

[51] S. K. Adhikari, A. C. Fonseca, and L. Tomio, Method for resonances and virtual states: Efimov virtual states, Phys. Rev. C **26**, 77 (1982).

[52] S. Bour, H.-W. Hammer, D. Lee, and U.-G. Meißner, Benchmark calculations for elastic fermion-dimer scattering, Phys. Rev. C **86**, 034003 (2012).

[53] J. von Stecher, C. H. Greene, and D. Blume, Energetics and structural properties of trapped two-component Fermi gases, Phys. Rev. A **77**, 043619 (2008).

[54] Experimental values are given in Ref. [25]. However, the original publication is S. J. Nikitin *et al.*, First Geneva Conf. **2**, 81 (1955) which, to the best of our efforts, we were not able to access.

[55] W. Gissler, Untersuchung des neutronenstreuquerschnittes von schwerem eis in der umgebung der braggschen grenzwellenlänge, Zeitschrift für Kristallographie **118**, 149 (1963).

[56] K. Schoen, D. L. Jacobson, M. Arif, P. R. Huffman, T. C. Black, W. M. Snow, S. K. Lamoreaux, H. Kaiser, and S. A. Werner, Precision neutron interferometric measurements and updated evaluations of the $n - p$ and $n - d$ coherent neutron scattering lengths, Phys. Rev. C **67**, 044005 (2003).

[57] I. N. Filikhin and S. L. Yakovlev, Microscopic calculation of low-energy deuteron-deuteron scattering on the basis of the cluster-reduction method, Phys. At. Nucl. **63**, 216 (2000).

[58] J. F. Carew, Deuteron-deuteron elastic and three- and four-body breakup scattering using the Faddeev-Yakubovski equations, Phys. Rev. C **103**, 014002 (2021).

[59] A. Deltuva, Universality in fermionic dimer-dimer scattering, Phys. Rev. A **96**, 022701 (2017).

[60] R. E. Donaldson, W. Bartolini, and H. Otsuki, Measurement of the coherent-scattering amplitude of tritium, Phys. Rev. C **5**, 1952 (1972).

[61] S. Hammerschmied, H. Rauch, H. Clerc, and U. Kischko, Measurements of the coherent neutron-tritium scattering length and its relation to the four nucleon problem, Z. Phys. A **302**, 323 (1981).

[62] H. Rauch, D. Tuppinger, H. Wölwitsch, and T. Wroblewski, Re-measurement of the neutron-tritium scattering length, Phys. Lett. B **165**, 39 (1985).

[63] T. W. Phillips, B. L. Berman, and J. D. Seagrave, Neutron total cross section for tritium, Phys. Rev. C **22**, 384 (1980).

[64] M. Viviani, S. Rosati, and A. Kievsky, Neutron-^{3}H and Proton-^{3}He Zero Energy Scattering, Phys. Rev. Lett. **81**, 1580 (1998).

[65] R. Lazauskas and J. Carbonell, *Ab initio* calculations of four-nucleon elastic scattering, Few-Body Syst. **34**, 105 (2004).

[66] M. Viviani, L. Girlanda, A. Kievsky, and L. E. Marcucci, $n + ^3$H, $p + ^3$He, $p + ^3$H, and $n + ^3$He scattering with the hyperspherical harmonic method, Phys. Rev. C **102**, 034007 (2020).

[67] G. M. Hale, D. C. Dodder, J. D. Seagrave, B. L. Berman, and T. W. Phillips, Neutron-triton cross sections and scattering lengths obtained from p-^{4}He scattering, Phys. Rev. C **42**, 438 (1990).

[68] H. Kaiser, H. Rauch, G. Badurek, W. Bauspiess, and U. Bonse, Measurement of coherent neutron scattering lengths of gases, Z. Phys. A **291**, 231 (1979).

[69] P. R. Huffman, D. L. Jacobson, K. Schoen, M. Arif, T. C. Black, W. M. Snow, and S. A. Werner, Precision neutron interferometric measurement of the $n - ^3$He coherent neutron scattering length, Phys. Rev. C **70**, 014004 (2004).

[70] W. Ketter, W. Heil, G. Badurek, M. Baron, E. Jericha, R. Loidl, and H. Rauch, Precision measurement of the coherent neutron scattering length of 3He through neutron interferometry, Eur. Phys. J. A **27**, 243 (2006).

[71] O. Zimmer, G. Ehlers, B. Farago, H. Humblot, W. Ketter, and R. Scherm, A precise measurement of the spin-dependent neutron scattering length of ^{3}He, Eur. Phys. J. Direct **4**, 1 (2002).

[72] M. G. Huber, M. Arif, T. C. Black, W. C. Chen, T. R. Gentile, D. S. Hussey, D. A. Pushin, F. E. Wietfeldt, and L. Yang, Precision Measurement of the n-^{3}He Incoherent Scattering Length Using Neutron Interferometry, Phys. Rev. Lett. **102**, 200401 (2009); **103**, 179903(E) (2009); M. G. Huber *et al.*, Neutron interferometric measurement of the scattering length difference between the triplet and singlet states of $n - ^3$He, Phys. Rev. C **90**, 064004 (2014).

[73] V. P. Alfimenkov, G. G. Akopyan, J. Wierzbicki, A. M. Govorov, L. B. Pikelner, and E. I. Sharapov, Neutron scattering lengths for ^{3}He, Yad. Fiz. **25**, 1145 (1977) [Sov. J. Nucl. Phys. **25**, 607 (1977)].

[74] H. M. Hofmann and G. M. Hale, Microscopic calculation of the spin-dependent neutron scattering lengths on ^{3}He, Phys. Rev. C **68**, 021002(R) (2003).

[75] H. Witała, A. Nogga, H. Kamada, W. Glöckle, J. Golak, and R. Skibiński, Modern nuclear force predictions for the neutron-deuteron scattering lengths, Phys. Rev. C **68**, 034002 (2003).

[76] R. Lazauskas (private communication).

[77] M. Viviani (private communication).

[78] W. G. Dawkins, J. Carlson, U. van Kolck, and A. Gezerlis, Clustering of Four-Component Unitary Fermions, Phys. Rev. Lett. **124**, 143402 (2020).

[79] M. Schäfer, L. Contessi, J. Kirscher, and J. Mareš, Multi-fermion systems with contact theories, Phys. Lett. B **816**, 136194 (2021).

[80] M. Eliyahu, B. Bazak, and N. Barnea, Extrapolating lattice QCD results using effective field theory, Phys. Rev. C **102**, 044003 (2020).

[81] W. Detmold and P. E. Shanahan, Few-nucleon matrix elements in pionless effective field theory in a finite volume, Phys. Rev. D **103**, 074503 (2021).

[82] A. Parreño, P. E. Shanahan, M. L. Wagman, F. Winter, E. Chang, W. Detmold, and M. Illa (NPLQCD Collaboration), Axial charge of the triton from lattice QCD, Phys. Rev. D **103**, 074511 (2021).

[83] R. Yaron, B. Bazak, M. Schäfer, and N. Barnea, Spectrum of light nuclei in a finite volume, Phys. Rev. D **106**, 014511 (2022).

[84] L. Contessi, N. Barnea, and A. Gal, Resolving the Λ Hypernuclear Overbinding Problem in Pionless Effective Field Theory, Phys. Rev. Lett. **121**, 102502 (2018).

[85] F. Hildenbrand and H.-W. Hammer, Three-body hypernuclei in pionless effective field theory, Phys. Rev. C **100**, 034002 (2019); **102**, 039901(E) (2020).

[86] F. Hildenbrand and H.-W. Hammer, Lifetime of the hypertriton, Phys. Rev. C **102**, 064002 (2020).

[87] M. Schäfer, B. Bazak, N. Barnea, A. Gal, and J. Mareš, Consequences of increased hypertriton binding for s-shell Λ-hypernuclear systems, Phys. Rev. C **105**, 015202 (2022), and earlier works listed therein.

[88] N. Barnea, B. Bazak, E. Friedman, and A. Gal, Onset of η-nuclear binding in a pionless EFT approach, Phys. Lett. B **771**, 297 (2017); **775**, 364 (2017).